sustainability

MDPI

Article

Flexibility-Constrained Energy Storage System Placement for Flexible Interconnected Distribution Networks

Zhipeng Jing [1], Lipo Gao [1], Yu Mu [2] and Dong Liang [2,*]

[1] Economic and Technological Research Institute, State Grid Hebei Electric Power Co., Ltd., Shijiazhuang 050021, China; jzp1506@163.com (Z.J.); gaotian7412@163.com (L.G.)
[2] State Key Laboratory of Reliability and Intelligence of Electrical Equipment, Hebei University of Technology, Tianjin 300401, China; 202221401119@stu.hebut.edu.cn
* Correspondence: liangdong@hebut.edu.cn

Abstract: Configuring energy storage systems (ESSs) in distribution networks is an effective way to alleviate issues induced by intermittent distributed generation such as transformer overloading and line congestion. However, flexibility has not been fully taken into account when placing ESSs. This paper proposes a novel ESS placement method for flexible interconnected distribution networks considering flexibility constraints. An ESS siting and sizing model is formulated aiming to minimize the life-cycle cost of ESSs along with the annual network loss cost, electricity purchasing cost from the upper-level power grid, photovoltaic (PV) curtailment cost, and ESS scheduling cost while fulfilling various security constraints. Flexible ramp-up/-down constraints of the system are added to improve the ability to adapt to random changes in both power supply and demand sides, while a fluctuation rate of net load constraints is also added for each bus to reduce the net load fluctuation. The nonconvex model is then converted into a second-order cone programming formulation, which can be solved in an efficient manner. The proposed method is evaluated on a modified 33-bus flexible distribution network. The simulation results show that better flexibility can be achieved with slightly increased ESS investment costs. However, a large ESS capacity is needed to reduce the net load fluctuation to low levels, especially when the PV capacity is large.

Keywords: energy storage system; optimal placement; flexible distribution network; flexibility constraint; flexible ramp-up/-down; fluctuation rate of net load

Citation: Jing, Z.; Gao, L.; Mu, Y.; Liang, D. Flexibility-Constrained Energy Storage System Placement for Flexible Interconnected Distribution Networks. *Sustainability* **2024**, *16*, 9129. https://doi.org/10.3390/su16209129

Academic Editor: John Bell

Received: 21 September 2024
Revised: 11 October 2024
Accepted: 18 October 2024
Published: 21 October 2024

1. Introduction

Distributed renewable energy resources (RESs) have continuously been installed into power distribution networks all over the world in recent years, mainly to reduce carbon emissions. Up to 2023, the cumulative installed capacity of distributed photovoltaic (PV) generation in China reached 254.438 GW. The integration of so much intermittent distributed generation brings serious issues for the secure operation of the distribution networks, such as transformer overloading and line congestion, but configuring energy storage systems (ESSs) is an effective way to alleviate these issues.

Considerable efforts have been devoted in the literature to ESS placement in distribution networks. In [1], the sizing and placement of the distribution grid connected battery systems is achieved using a second-order cone-convex relaxation of the power flow equations. In [2], a hierarchical planning model is proposed for battery ESS (BESS) configurations, including three interacting levels: determination of the optimal BESS number, selection of the most effective locations for a given BESS number based on voltage sensitivity analysis, and sizing the BESS capacity to minimize the investment cost, residual value of BESS, and system operation cost. In [3], a multi-objective BESS placement model is proposed for unbalanced distribution networks to minimize the costs of primary investment and operation/maintenance while maximizing the savings by loss reduction and load shifting. A sequential BESS placement strategy is presented based on a loss

sensitivity index. In [4], an ESS planning method is proposed for distribution grids to see if curtailing PV generation might be more economical than installing an ESS. The problem minimizes the net investment costs of the ESSs and the imported and exported electricity costs while modeling the power grid constraints by linearized power flow equations to keep the problem formulation tractable.

Scenario-based stochastic programming is usually used to handle variations in RESs and loads. In [5], a trilevel ESS planning formulation with min–max risk constraints is developed considering that the siting choice of individual RES owners could conflict with the system operation targets of hosting capacity improvement. The stochastic model is solved using a customized column-and-constraint generation algorithm. In [6], an ESS siting and sizing method is proposed for distribution networks embedding seasonal network reconfiguration. The model aims to minimize voltage magnitude deviations, feeder/line congestion, cost of supplying loads, and investment costs related to the ESSs, using a conditionally exact convex optimal power flow. Benders' decomposition algorithm is used to solve the stochastic model. In [7], a distributed BESS planning method is presented leveraging model predictive control strategies [8,9] using Benders' decomposition technique. The objective is to maximize PV utilization and minimize battery degradation while satisfying all grid constraints. In [10], an ESS siting and sizing method is presented to minimize the dispatch error at the connecting point to the upper-layer grid, using Benders' decomposition technique and an augmented relaxed optimal power flow model, which is proven to provide a global optimal and exact solution in the case of radial power grids. In [11], the optimal allocation of BESS is proposed to minimize the investment and maintenance costs of the BESS, the operation cost of the whole system, and the loss cost of the whole system. The BESS location is first determined based on the calculated adjusted voltage violation risk, and then the capacity of the BESS is obtained via a supervised learning-based power flow. In [12], a two-stage mixed-integer linear programming problem is formulated that determines the capacity, number of discharge cycles of batteries in the first stage, and lifetime of the battery based on the partial depth of discharge in the second stage. The uncertainty of PV and demand are taken into account through probabilistic analysis and time-period clustering.

Robust optimization is another way to handle uncertain parameters. In [13], an adaptive robust optimization model with integer recourse variables is proposed for BESS allocation to reduce the power imbalance and alleviate the voltage increase, regarding future PV installations determined by customers as uncertainties. The model is solved using a modified column-and-constraint generation algorithm. In [14], a robust distributed BESS planning model is expressed by minimizing the difference among the BESS planning, degradation, operation costs, and the revenue of BESS from selling its stored energy. An equivalent linear programming model is proposed using the first-order expansion of Taylor's series for linearization of power flow equations and a polygon for linearization of circular inequalities. The bounded uncertainty set is used to model the uncertain parameters including forecasted loads, charging/discharging prices, and output power of RESs.

Various factors other than security constraints are also considered for ESS placement including reliability and resilience, power quality, and operation flexibility. From the perspective of reliability and resilience, in [15], a planning framework is introduced for ascertaining the most cost-effective siting and sizing of ESSs that maximize their benefits in distribution networks. Contingency planning decisions, in the form of load points to be shed during contingencies, are identified. In [16], a multistage stochastic model is developed to determine the optimal sizing, timing, and placement of distributed generators in coordination with ESSs and reactive power sources. The problem is formulated as a mixed-integer linear programming optimization using a linearized AC network model to minimize the total costs corresponding to investment, maintenance, operation, reliability, and emission. In [17], a BESS placement method in radial distribution networks is proposed and is mainly intended for improving the reliability. The method uses utility historical load, outage, and project-cost data and relies on a mixed-integer linear programming

optimization tool. In [18], a mixed-integer linear programming model is developed to optimally determine the size and site of a BESS connected to the distribution network for peak shaving and reliability improvement, under both normal and outage scenarios. In [19], RESs, stationary BESSs, and power electric vehicle parking lots are co-planned under normal and resilient operation to restore prioritized loads while meeting topological and operational constraints. Demand response programs and interruptible loads are introduced to enhance the resilience of distribution systems. From the perspective of power quality, in [20], an optimal allocation strategy is proposed for distributed ESSs in distribution networks to simultaneously minimize voltage deviation, flickers, power losses, and line loading. In [21], the co-planning of wind turbines and ESSs is formulated to minimize flicker emission and voltage deviation produced by wind turbines in addition to power losses and ESS costs. From the perspective of operation flexibility, in [22], a two-stage model is developed to site and size a BESS in a distribution network to provide local flexibility services for the distribution system operator and frequency containment reserve for the transmission system operator. The first stage allocates the battery to managing congestions or interruptions of supply and ensures reliable electricity supply in the local distribution network. The second stage optimally sizes the BESS to boost the profit by providing a frequency containment reserve for normal operation.

In summary, ESS placement has been studied from various perspectives. Recently, maintaining the operational flexibility of distribution systems has become an important focus primarily because of the increased levels of grid-connected, variable renewable energy, as well as changing customer behaviors on the distribution side. However, flexibility has not been fully taken into account when placing ESSs. This paper proposes a novel flexibility-constrained ESS placement method for flexible interconnected distribution networks. The contributions are summarized as follows:

(1) A novel ESS siting and sizing model is formulated aiming to minimize the life-cycle cost of ESSs along with the annual network loss cost, electricity purchasing cost from the upper-level power grid, PV curtailment cost, and ESS scheduling cost while fulfilling security constraints.
(2) Flexible ramp-up/-down constraints of the system are added to improve the ability to adapt to random changes in both power supply and demand sides, while the fluctuation rate of net load constraints is also added for all buses to reduce the net load fluctuation.
(3) The nonconvex model is transformed into a second-order cone programming formulation, enabling it to be solved efficiently. The proposed method is thoroughly evaluated on a modified 33-bus flexible distribution network. Various sensitivity analyses are conducted under different user preferences on flexibility degrees.

The remainder of this paper is organized as follows: Section 2 presents the models of flexibility resources. Section 3 presents the proposed flexibility-constrained ESS placement method. Section 4 describes the simulation results, and conclusions are drawn in Section 5.

2. Modeling of Flexibility Resources and Flexibility Evaluation

2.1. Modeling of Flexible Resources in Distribution Systems

Generally speaking, all types of controllable resources can be treated as flexible resources, including ESSs, distributed generation (DG) inverters, reactive power compensation devices, flexible distribution switches (FDSs), network reconfiguration, on-load tap changers, electric vehicles, and interruptible loads due to their ability to control power flow. As we mainly focus on the real power balance problem, reactive power compensation devices are not considered. Network reconfiguration and on-load tap changers cannot be frequently regulated and are also not discussed in this paper. FDSs, ESSs, and DG inverters are considered as flexible resources in the formulation of ESS placement.

2.1.1. Steady-State Operation Model of FDSs

A typical multi-terminal FDS consists of multiple back-to-back voltage source converters (VSCs), as shown in Figure 1. In normal operation mode, the control variables of an FDS consist of the real and reactive power delivered by each VSC. Assuming the power injection into the grid to be the positive direction and neglecting power losses, the following constraints should be fulfilled for each FDS:

$$\sum_{i \in \Omega_{b(v)}} P_{i,t,\mathrm{FDS}} = 0 \tag{1}$$

$$\sqrt{(P_{i,t,\mathrm{FDS}})^2 + (Q_{i,t,\mathrm{FDS}})^2} \leq S_{\max,\mathrm{FDS}}, \forall i \in \Omega_{b(v)} \tag{2}$$

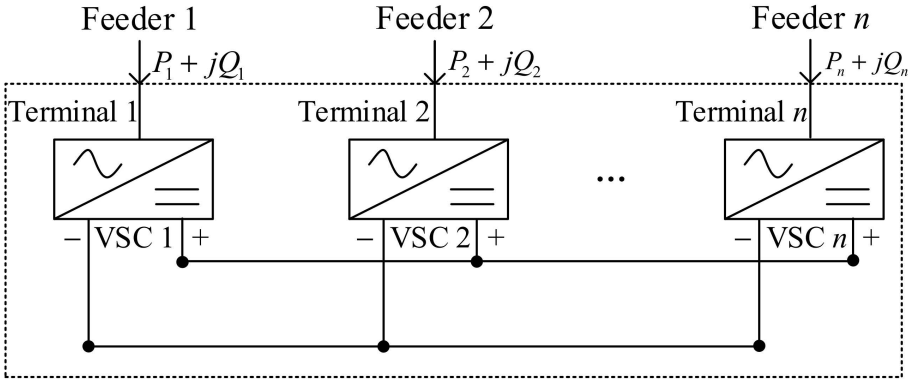

Figure 1. Illustration of the back-to-back multi-terminal FDS.

Constraint (1) is let the sum of real power injection from all VSCs be zero. Constraint (2) is let the apparent power flow through each VSC be less than each VSC's capacity.

2.1.2. Steady-State Operation Model of ESSs

The following constraints should be fulfilled for each ESS:

$$\mu_{i,t}^{+} + \mu_{i,t}^{-} \leq 1 \tag{3}$$

$$0 \leq P_{i,t,\mathrm{ESS}}^{+} \leq \mu_{i,t}^{+} P_{Ri,\mathrm{ESS}} \tag{4}$$

$$0 \leq P_{i,t,\mathrm{ESS}}^{-} \leq \mu_{i,t}^{-} P_{Ri,\mathrm{ESS}} \tag{5}$$

$$E_{i,t} = E_{i,t-1} + \eta_i^c P_{i,t,\mathrm{ESS}}^{+} \Delta t - (1/\eta_i^d) P_{i,t,\mathrm{ESS}}^{-} \Delta t \tag{6}$$

$$E_{Ri,\mathrm{ESS}} SOC_{\min} \leq E_{i,t} \leq E_{Ri,\mathrm{ESS}} \cdot SOC_{\max} \tag{7}$$

$$E_{i,0} = E_{i,T} \tag{8}$$

$$\sum_{t \in \Omega_T} P_{i,t,\mathrm{ESS}}^{loss} = \sum_{t \in \Omega_T} (P_{i,t,\mathrm{ESS}}^{+} - P_{i,t,\mathrm{ESS}}^{-}) \tag{9}$$

Constraint (3) is avoid ESSs simultaneously charging and discharging. Constraints (4) and (5) are let the charging/discharging power be less than the ESS's capacity. Constraint (6) is let the ESS's energy satisfy the continuity constraint. Constraint (7) is avoid overcharging and overdischarging for ESSs. Constraint (8) is let the final energy at the end of the whole period be equal to the initial energy. Constraint (9) is describe the energy losses of each ESS.

To mitigate the model complexity induced by the binary variables, the losses of the ESSs are not discussed in this paper, and the ESS constraints become the following:

$$0 \leq P_{i,t,\mathrm{ESS}} \leq P_{Ri,\mathrm{ESS}} \tag{10}$$

$$E_{Ri,\mathrm{ESS}} SOC_{\min} \leq E_{i,t} \leq E_{Ri,\mathrm{ESS}} \cdot SOC_{\max} \tag{11}$$

$$E_{i,0} = E_{i,T} \tag{12}$$

$$E_{i,t} = E_{i,t-1} - P_{i,t,\mathrm{ESS}}\Delta t \tag{13}$$

In constraints (10) and (13), the approximate discharging power $P_{i,t,\mathrm{ESS}}$ is introduced such that a positive value indicates the ESS is discharging and a negative value indicates the ESS is charging.

2.1.3. Steady-State Operation Model of DG Inverters

While most of the time DG inverters work in the mode of maximum power point tracking, superfluous real power can be curtailed to mitigate the overvoltage issues as follows:

$$0 \le P^{\mathrm{cut}}_{i,t,\mathrm{DG}} \le P_{i,t,\mathrm{DG}} \tag{14}$$

2.2. Flexibility Definition and Indices

2.2.1. Flexibility Definition

Power system flexibility can be defined as the ability to adapt to random changes in both power supply and demand sides within a time period by coordinating various flexible resources. In this paper, the flexibility is modeled through the calculation of flexible ramp requirements of each bus in each dispatch interval, as shown in Figure 2 [23], which is assumed to be the net load curve of a distribution substation bus.

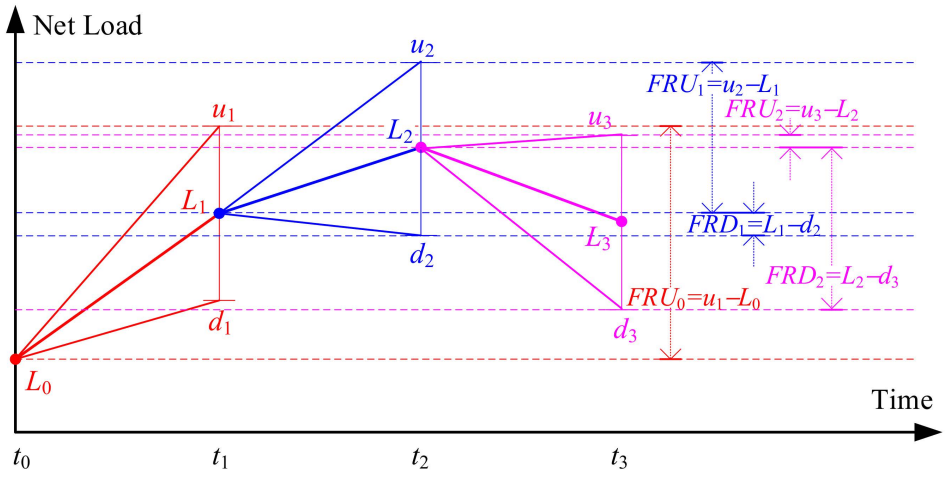

Figure 2. Ramp requirements considering net load variability and uncertainty.

(1) At time t_0, the current net load is L_0. The forecasted value and the upper and lower bounds of the net load at time t_1 are L_1, u_1, and d_1, respectively. As $d_1 > L_0$, we inferred that there is only a flexible ramp-up (FRU) requirement without a flexible ramp-down (FRD) requirement. The FRU requirement FRU_0 is equal to u_1-L_0, taking the forecasting uncertainty into account.

(2) At time t_1, the current net load is L_1. The forecasted value and the upper and lower bounds of the net load at time t_2 are L_2, u_2, and d_2, respectively. As $d_2 < L_1 < u_2$, we inferred that there is both an FRU requirement and an FRD requirement. FRU_1 is equal to u_2-L_1, and FRD_1 is equal to L_1-d_2, taking the forecasting uncertainty into account.

(3) Similarly, at time t_2, the current net load is L_2. The forecasted value and the upper and lower bounds of net load at time t_3 are L_3, u_3, and d_3, respectively. As $d_3 < L_2 < u_3$, there is both an FRU requirement and an FRD requirement. FRU_2 is equal to u_3-L_2, and FRD_2 is equal to L_2-d_3.

2.2.2. Flexibility Capability

Flexible ramp-up and flexible ramp-down indices of an ESS are defined as follows:

$$FRU_{i,t,\mathrm{ESS}} = \min\left\{P_{Ri,\mathrm{ESS}} - P_{i,t,\mathrm{ESS}}, \frac{E_{i,t} - E_{Ri,\mathrm{ESS}}SOC_{\min}}{\Delta t}\right\} \tag{15}$$

$$FRD_{i,t,\mathrm{ESS}} = \min\left\{P_{i,t,\mathrm{ESS}} + P_{Ri,\mathrm{ESS}}, \frac{E_{Ri,\mathrm{ESS}} \cdot SOC_{\max} - E_{i,t}}{\Delta t}\right\} \tag{16}$$

Flexible ramp-up and flexible ramp-down indices of a DG inverter are defined as follows:

$$FRU_{i,t,\mathrm{DG}} = P^{\mathrm{cut}}_{i,t,\mathrm{DG}} \tag{17}$$

$$FRD_{i,t,\mathrm{DG}} = P_{i,t,\mathrm{DG}} - P^{\mathrm{cut}}_{i,t,\mathrm{DG}} \tag{18}$$

Flexible ramp-up and flexible ramp-down indices of the whole system are defined as follows:

$$FRU_t = \sum_{i\in\Omega_{\mathrm{ESS}}} FRU_{i,t,\mathrm{ESS}} + \sum_{i\in\Omega_{\mathrm{DG}}} FRU_{i,t,\mathrm{DG}} \tag{19}$$

$$FRD_t = \sum_{i\in\Omega_{\mathrm{ESS}}} FRD_{i,t,\mathrm{ESS}} + \sum_{i\in\Omega_{\mathrm{DG}}} FRD_{i,t,\mathrm{DG}} \tag{20}$$

2.2.3. Flexibility Requirement

Neglecting the forecasting uncertainties in Figure 2 for our ESS planning task, flexible ramp-up/-down requirements of the whole system are defined as follows:

$$URR_{i,t} = \max\{P_{i,t+1,\mathrm{NET}} - P_{i,t,\mathrm{NET}}, 0\} \tag{21}$$

$$DRR_{i,t} = \max\{P_{i,t,\mathrm{NET}} - P_{i,t+1,\mathrm{NET}}, 0\} \tag{22}$$

Flexible ramp-up/-down requirements of the whole system are defined as follows:

$$URR_t = \sum_{i\in\Omega_b\setminus\{root\}} URR_{i,t} \tag{23}$$

$$DRR_t = \sum_{i\in\Omega_b\setminus\{root\}} DRR_{i,t} \tag{24}$$

2.2.4. Fluctuation Rate of Net Load

Another index that is used for flexibility evaluation is the fluctuation rate of net load (FRNL), which is defined as the ratio of the real net power's standard deviation with respect to the distribution transformer's capacity:

$$FRNL_i = \frac{\sigma_i}{S_{Ti}} \times 100\% \tag{25}$$

$$\sigma_i = \sqrt{\frac{\sum\limits_{t\in\Omega_T} \left(P_{i,t} - \overline{P}_i\right)^2}{T}} \tag{26}$$

$$\overline{P}_i = \frac{1}{T}\sum_{t\in\Omega_T} P_{i,t} \tag{27}$$

3. Flexibility-Constrained ESS Placement

3.1. Fundamental Formulation

3.1.1. Objective Function

The objective is to minimize the annual total cost, including the equivalent annual investment cost of ESSs and the annual operation and maintenance costs of the system.

$$\min C_{\text{Total}} = C_{\text{EAI}} + 365 * C_{\text{OM}} \tag{28}$$

The equivalent annual investment cost of ESSs is

$$C_{\text{EAI}} = \sum_{i \in \Omega_{\text{ESS}}} \frac{r(1+r)^y}{(1+r)^y - 1} (c_e E_{Ri,\text{ESS}} + c_p P_{Ri,\text{ESS}}) \tag{29}$$

The annual operation and maintenance costs of the system is

$$C_{\text{OM}} = C_{\text{NLC}} + C_{\text{PRC}} + C_{\text{PC}} + C_{\text{FRSC}} \tag{30}$$

C_{NLC}, C_{PRC}, C_{PC}, and C_{FRSC} are calculated as

$$C_{\text{NLC}} = c_{loss} \sum_{t \in \Omega_T} \sum_{i \in \Omega_b} P_{i,t} \Delta t \tag{31}$$

$$C_{\text{PRC}} = c_g \sum_{t \in \Omega_T} P_t^{\text{g}} \Delta t \tag{32}$$

$$C_{\text{PC}} = c_{ap} \sum_{t \in \Omega_T} \sum_{k \in \Omega_{\text{DG}}} P_{k,t}^{\text{ap}} \Delta t \tag{33}$$

$$C_{\text{FRSC}} = c_{ess} \sum_{t \in \Omega_T} \sum_{i \in \Omega_{\text{ESS}}} |P_{i,t,\text{ESS}}| \Delta t \tag{34}$$

3.1.2. FDS Constraints

Constraints (1) and (2) should be added as constraints for FDSs.

3.1.3. ESS Constraints

In addition to ESS constraints, the following constraint is added to limit the maximum continuous working time of each ESS to 2 h:

$$E_{Ri,\text{ESS}} = 2 P_{Ri,\text{ESS}} \tag{35}$$

3.1.4. DG Inverter Constraint

Constraints (14) should be added as constraints for DG Inverters.

3.1.5. Flexibility Constraints

Three flexibility constraints are added as follows:

$$FRU_t \geq URR_t, \quad t \in \{1, \cdots, T-1\} \tag{36}$$

$$FRD_t \geq DRR_t, \quad t \in \{1, \cdots, T-1\} \tag{37}$$

$$FRNL_i \leq FRNL_{set}, \quad i \in \Omega_b \tag{38}$$

Constraint (36) is let the FRU capability be larger than the FRU requirement for all time intervals. Constraint (37) is let the FRD capability be larger than the FRD requirement for all time intervals. Constraint (38) is let the FRNL index of all buses be less than a pre-set threshold $FRNL_{set}$.

3.1.6. Power Flow Constraints

According to the DistFlow model, the power flow constraints are as follows:

$$P_{i,t} = P_{i,t,\mathrm{DG}} - P^{\mathrm{cut}}_{i,t,\mathrm{DG}} - P_{i,t,\mathrm{L}} + P_{i,t,\mathrm{FDS}} + P_{i,t,\mathrm{ESS}} \tag{39}$$

$$Q_{i,t} = -Q_{i,t,\mathrm{L}} + Q_{i,t,\mathrm{FDS}} \tag{40}$$

$$\sum_{(k,i)\in\Omega_l} (P_{ki,t} - I^2_{ki,t} r_{ki}) - \sum_{(i,j)\in\Omega_l} P_{ij,t} = -P_{i,t} \tag{41}$$

$$\sum_{(k,i)\in\Omega_l} (Q_{ki,t} - I^2_{ki,t} x_{ki}) - \sum_{(i,j)\in\Omega_l} Q_{ij,t} = -Q_{i,t} \tag{42}$$

$$V^2_{j,t} = V^2_{i,t} - 2(P_{ij,t} r_{ij} + Q_{ij,t} x_{ij}) + (r^2_{ij} + x^2_{ij}) I^2_{ij,t} \tag{43}$$

$$P^2_{ij,t} + Q^2_{ij,t} = V^2_{i,t} I^2_{ij,t} \tag{44}$$

Constraints (39) and (40) describe the real and reactive power injection of each bus. Constraints (41) and (42) let each non-slack bus satisfy the power balance equation. Constraint (43) is the voltage drop constraint for each line. Quadratic constraint (44) describes the relation among real, reactive power flow current magnitude, and voltage magnitude at the start bus, which should be satisfied for each line.

3.1.7. Security Constraints

The voltage magnitude of each bus should be within the secure bounds:

$$V_{\min} \le V_{i,t} \le V_{\max} \tag{45}$$

The current magnitude of each line should not exceed the line's thermal limit:

$$0 \le I_{ij,t} \le I_{ij,\max} \tag{46}$$

3.2. Model Reformulation

Due to the nonconvexity of power flow constraints, the fundamental formulation is a nonconvex problem which is generally NP-hard. In this section, the problem is converted into a second-order cone programming problem, which can be efficiently solved using existing mature solvers.

3.2.1. Second-Order Cone Relaxation

We defined auxiliary variables $u_{i,t}, w_{ij,t}$ to replace $V^2_{i,t}$, $I^2_{ij,t}$, and using the second-order relaxation, the power flow constraints (41)–(43) are reformulated as follows:

$$\sum_{(k,i)\in\Omega_l} (P_{ki,t} - w_{ki,t} r_{ki}) - \sum_{(i,j)\in\Omega_l} P_{ij,t} = -P_{i,t} \tag{47}$$

$$\sum_{(k,i)\in\Omega_l} (Q_{ki,t} - w_{ki,t} x_{ki}) - \sum_{(i,j)\in\Omega_l} Q_{ij,t} = -Q_{i,t} \tag{48}$$

$$u_{j,t} = u_{i,t} - 2(P_{ij,t} r_{ij} + Q_{ij,t} x_{ij}) + (r^2_{ij} + x^2_{ij}) w_{ij,t} \tag{49}$$

Constraint (44) is reformulated as the following second-order cone constraint:

$$\left\| \begin{bmatrix} 2P_{ij,t} & 2Q_{ij,t} & w_{ij,t} - u_{i,t} \end{bmatrix}^{\mathrm{T}} \right\|_2 \le w_{ij,t} + u_{i,t} \tag{50}$$

Accordingly, constraints (45) and (46) become the following:

$$(V_{\min})^2 \le u_{i,t} \le (V_{\max})^2 \tag{51}$$

$$0 \le w_{ij,t} \le (I_{ij,\max})^2 \tag{52}$$

3.2.2. Variance Replacement

The variance format in (25)–(27) and the corresponding flexibility constraint are reformulated as the following linear constraints:

$$P_{i,t} - \overline{P}_i \le \sigma_i, \quad i \in \Omega_b \tag{53}$$

$$-P_{i,t} + \overline{P}_i \le \sigma_i, \quad i \in \Omega_b \tag{54}$$

$$\frac{\sigma_i}{S_{Ti}} \le FRNL_{set}, \quad i \in \Omega_b \tag{55}$$

Constraints (53) and (54) limit the deviation of real power injection during each time interval from the average value of all time periods. Constraint (55) limits the fluctuation rate of the net load at each bus.

4. Simulation Results

In this section, the proposed method is evaluated on the modified flexible interconnected 33-bus distribution network, as shown in Figure 3. A three-terminal FDS is configured to connect buses 18, 22, and 33. Ten PVs are placed at buses 3, 6, 9, 12, 15, 18, 21, 24, 27, and 30. The parameters needed for ESS placement are listed in Table 1.

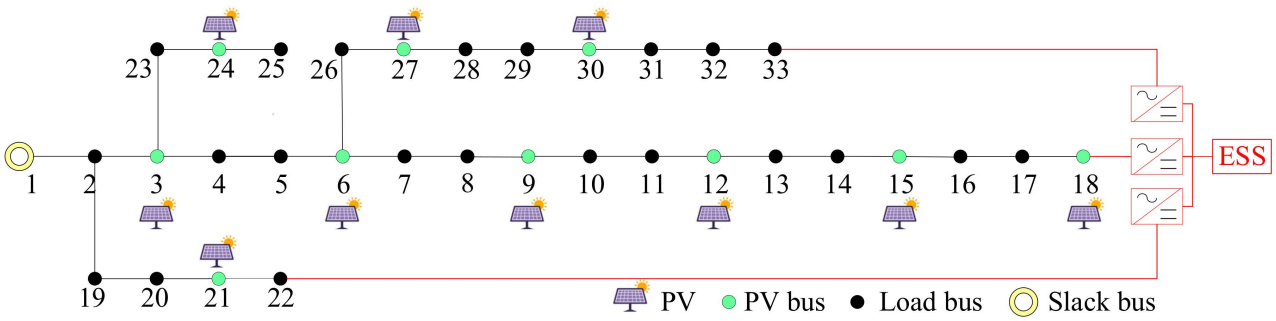

Figure 3. The 33-bus distribution network.

Table 1. Parameter values.

Parameter	Value	Parameter	Value
c_e	1270 CNY/kWh	c_g	0.6 CNY/kWh
c_p	1650 CNY/kWh	c_{ap}	0.6 CNY/kWh
y	10 years	c_{ess}	0.08 CNY/kWh
r	0.1	S_{T1}	6.3 MVA
c_{loss}	0.6 CNY/kWh	$S_{T2\sim33}$	800 kVA

Actual real, reactive loads from 26 distribution substations are used. The data are measured every 15 min for three consecutive months (May, June, and July, 2019), resulting in 8732 data points for each distribution substation. By selecting one typical day with the heaviest load burden, 32 96-point load curves are extracted, normalized to 0~1, and randomly allocated to buses of the 33-bus network. Similarly, actual 96-point PV generation data points of one typical day are normalized to 0~1 and allocated to the 10 PVs. The load coefficient curves of 32 buses and the PV coefficient curve used for simulation are shown in Figure 4.

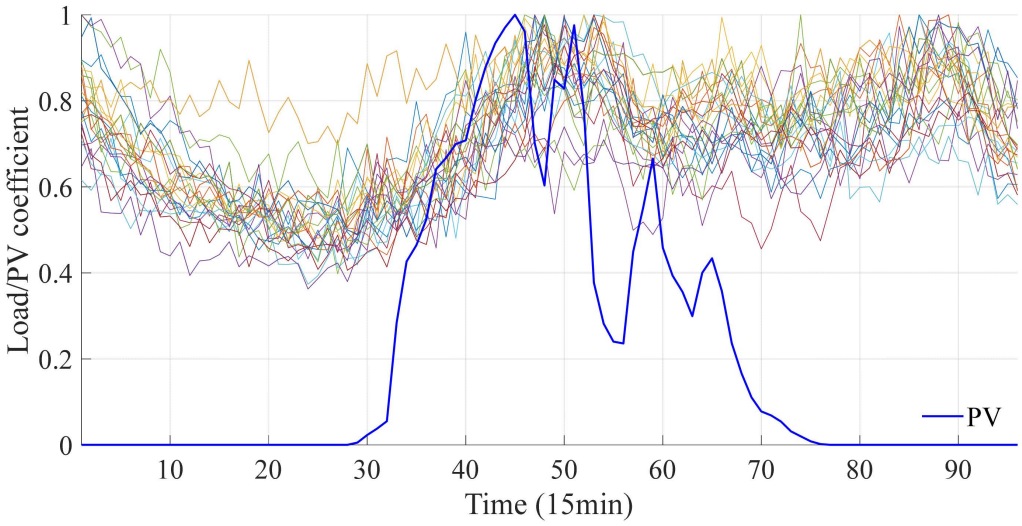

Figure 4. The load coefficient curves of 32 buses and the PV coefficient curve.

The installation capacities of 10 PVs are set the same as 100 kW, 200 kW, 300 kW, 400 kW, and 500 kW, resulting in a whole PV capacity of 1~5 MW. The proposed ESS placement formulation is tested under different $FRNL_{set}$ constraints and PV capacities. Two scenarios are compared as follows, and the results are analyzed in the following sections:

(1) Scenario 1: ESS placement without the FRU/FRD constraints in (15);
(2) Scenario 2: Flexibility-constrained ESS placement with the FRU/FRD constraints in (15) (termed "FC" hereinafter).

In order to reflect the impact of the collaborative effect of flexible resources in distribution networks on ESS configuration, cutting PV power generation through inverters is allowed as a reasonable manner for PV stations to participate in grid regulation, such that voltage/current violations can be eliminated. We can focus on the economic costs corresponding to the curtailed power generation.

4.1. Cost Analysis

The C_{EAI}, C_{OM}, and C_{Total} curves under different $FRNL_{set}$s and PV capacities are shown in Figure 5. It can be seen that the annual investment cost and the total annual cost increases as we tighten the $FRNL_{set}$ constraint, and a sudden increasement can be observed as the $FRNL_{set}$ decreases below a threshold. For example, when 300 kW PV generation is installed at the 10 PV buses, the total cost suddenly increases as the $FRNL_{set}$ decreases to 50%. These turning points provide effective references for PV planning: (1) when the PV installation capacity is low (100 kW, for example), the net load fluctuation level is also very low such that no extra investment of ESS is needed; (2) when the PV installation capacity increases (500 kW for example), huge investment costs of ESS are needed to suppress net load fluctuation to an acceptable level. Therefore, installing more than 5 MW of PV generation seems not economic for this system as the investment cost to avoid transformer overloading will be very large. In addition, the investment costs and operation/maintenance costs increase slightly when flexibility is added.

The C_{NLC}, C_{PRC}, C_{PC}, and C_{FRSC} curves under different $FRNL_{set}$s and PV capacities are shown in Figure 6. It can be seen that as we tighten the $FRNL_{set}$ constraint, the annual network loss cost first increases and then decreases when flexibility is dropped. For example, when the PV installation capacity is 200 kW, the peak of C_{NLC} appears at $FRNL_{set}$ = 70%. This is because as $FRNL_{set}$ starts decreasing, no extra ESSs are placed (which can be observed from Figure 5a), but more PV generation is curtailed, resulting in more power delivered from the upper-level power grid and thus more network loss. During this stage, curtailing PV generation is more economic than installing ESSs. After the peak of C_{NLC}, installing

ESSs becomes more economic than curtailing PV generation, resulting in more consumption of PV generation, less power delivered from the upper-level power grid, and thus less network loss. This explanation can be supported by Figure 5c, where PV curtailment costs first increase and then decrease. On the other side, when we add the FRU/FRD constraints, this phenomenon disappears; i.e., both network loss costs and PV curtailment costs decrease as we tighten the $FRNL_{set}$ constraint. This is because with the FRU/FRD constraints, there are always ESSs installed and the local consumption of PV generation first remains unchanged and then increases monotonically, resulting in fewer network loss costs and PV curtailment costs. In addition, the scheduling costs of ESSs increase rapidly as we tighten the $FRNL_{set}$ constraint, which indicates that the ESSs are much more frequently scheduled to reduce the net load fluctuation.

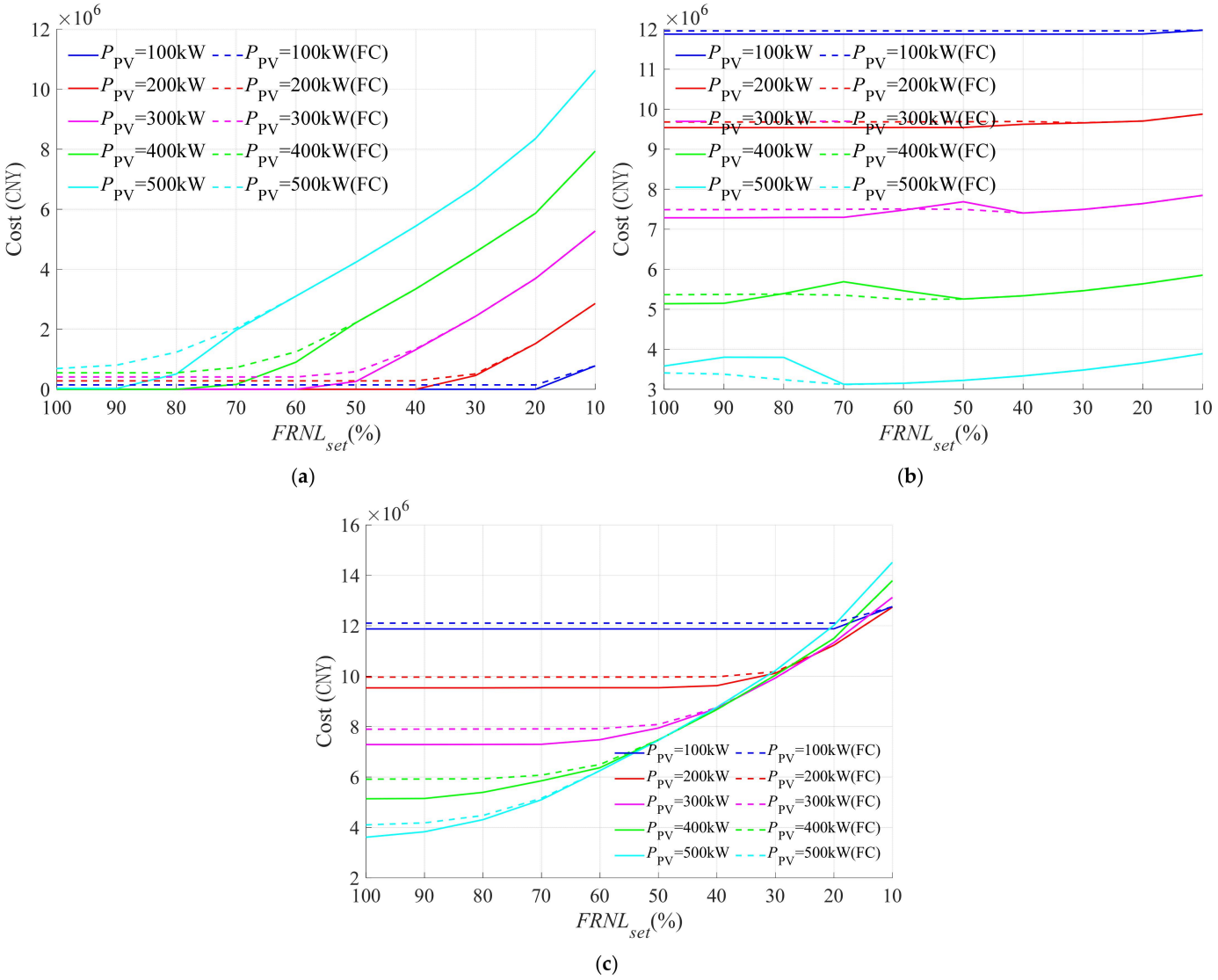

Figure 5. C_{EAI}, C_{OM}, and C_{Total} curves under different $FRNL_{set}$s and PV capacities. (**a**) C_{EAI} curves; (**b**) C_{OM} curves; (**c**) C_{Total} curves.

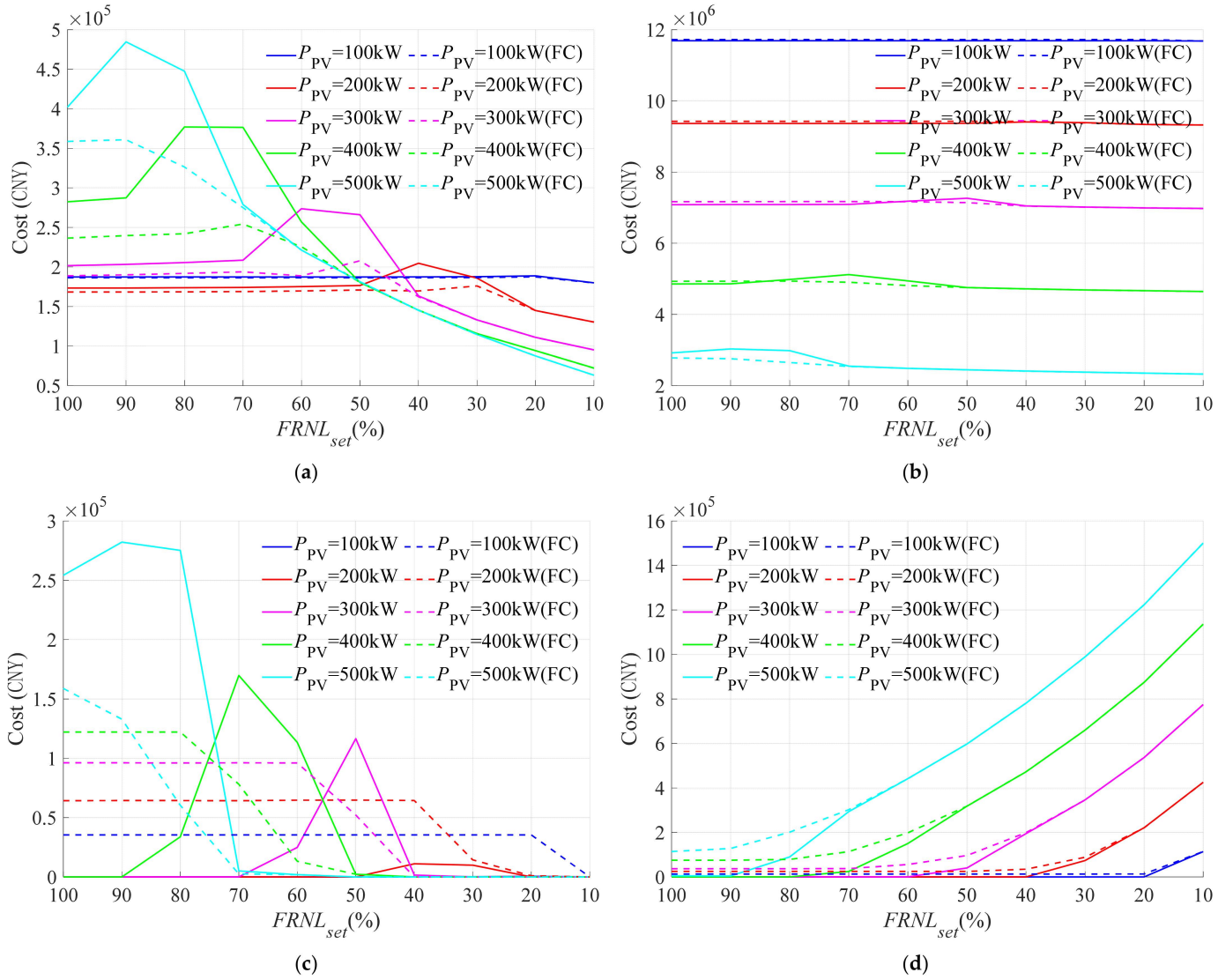

Figure 6. C_{NLC}, C_{PRC}, C_{PC}, and C_{FRSC} curves under different $FRNL_{set}$s and PV capacities. (**a**) C_{NLC} curves; (**b**) C_{PRC} curves; (**c**) C_{PC} curves; (**d**) C_{FRSC} curves.

4.2. Flexibility Analysis

The FRU/FRD capabilities and requirements when P_{PV} = 200 kW and $FRNL_{set}$ = 60% are shown in Figure 7. It can be seen that when the FRU/FRD constraints are dropped, the flexible FRU/FRD requirements cannot be fulfilled during some time intervals. At the same time, with the FRU/FRD constraints added, the FRU/FRD requirements can always be fulfilled during the whole day.

The real power injection curves under different $FRNL_{set}$s and PV capacities are shown in Figure 8. The results when the FRU/FRD constraints are dropped are displayed in the illustration. It can be seen that as we tighten the $FRNL_{set}$ constraint, the net load becomes increasingly flatter, which shows the capability of placing ESSs to dramatically reduce net load volatility and delay expansion investment of larger-capacity transformers.

4.3. ESS Capacity Analysis

The total ESS installation capacities under different $FRNL_{set}$s and PV capacities are shown in Figure 9, and the detailed ESS configurations of all buses are displayed in Figure 10. It can be seen that most of the ESSs are installed at buses where PVs are installed except bus 18, which is interconnected with other laterals through a three-terminal FDS. As expected, the ESS capacity increases quickly as we tightened the $FRNL_{set}$ constraint,

indicating that a large ESS capacity is needed to reduce the net load fluctuation to low levels, especially when the PV capacity is large. Another observation is that ESSs are not placed at the substation bus 1, indicating that the idea of hierarchically placing ESSs through a centralized ESS at the substation and other distributed local ESSs is not economically preferable.

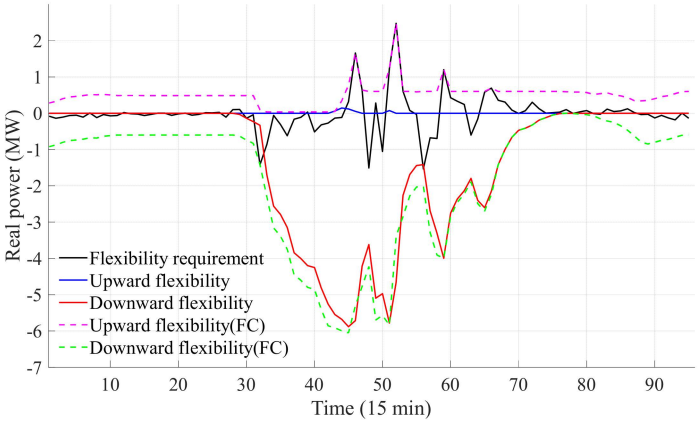

Figure 7. FRU/FRD capabilities and requirements (P_{PV} = 200 kW and $FRNL_{set}$ = 60%).

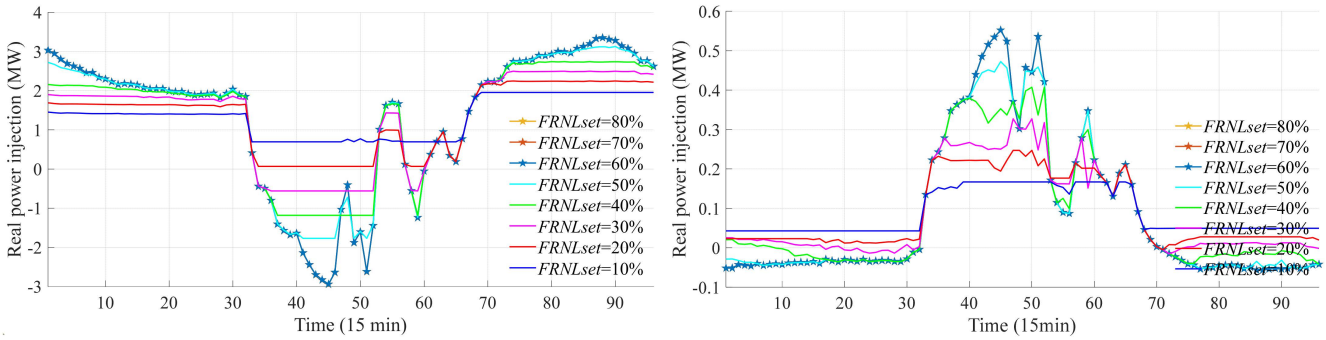

(**a**) (**b**)

Figure 8. Real power injection curves under different $FRNL_{set}$s and PV capacities. (**a**) The root bus and (**b**) PV bus 15.

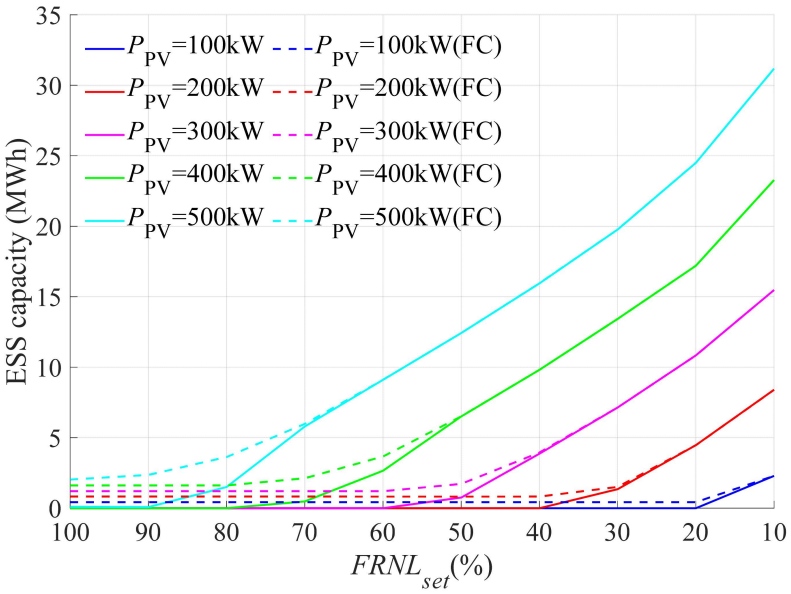

Figure 9. Total ESS installation capacities under different $FRNL_{set}$s and PV capacities.

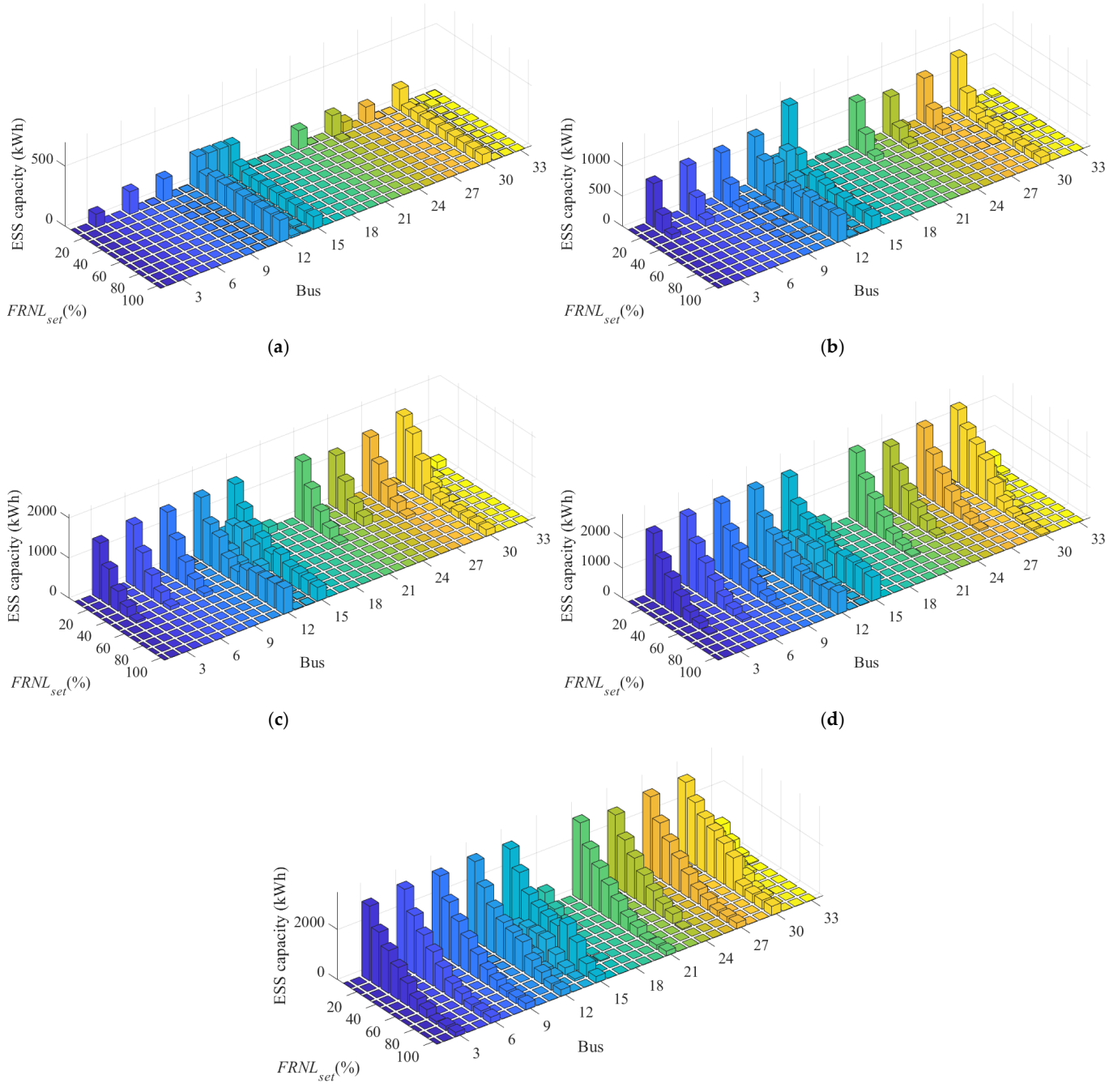

Figure 10. Detailed ESS configurations of all buses under different $FRNL_{set}$s and PV capacities. (**a**) P_{PV} = 100 kW for each PV bus; (**b**) P_{PV} = 200 kW for each PV bus; (**c**) P_{PV} = 300 kW for each PV bus; (**d**) P_{PV} = 400 kW for each PV bus. (**e**) P_{PV}=500kW for each PV bus.

4.4. Limitations

Although acceptable simulation results are obtained in a very efficient manner, two limitations are summarized as follows:

(1) The ESS constraints are simplified by neglecting the different losses during charging and discharging, which may introduce bias from realistic situation.
(2) Only one typical scenario is selected for load and solar generation, which may make the ESS siting and sizing decision incapable of handling various loading conditions and solar generation scenarios.

5. Conclusions

To alleviate issues induced by intermittent distributed generation, such as transformer overloading and line congestion, a novel ESS placement method is proposed for flexible interconnected distribution networks considering flexibility constraints. An ESS siting and sizing model is formulated aiming to minimize the life-cycle cost of ESSs along with the annual network loss cost, electricity purchasing cost from the upper-level power grid, PV curtailment cost, and ESS scheduling cost, while fulfilling various security constraints. A fluctuation rate of net load constraints is also added for all buses to reduce the net load fluctuation.

The proposed method is evaluated on a modified 33-bus flexible distribution network with various sensitivity analysis, and the following conclusions are drawn:

(1) Inclusion of the fluctuation rate of net load constraint provides an intuitive reference for planners to evaluate and improve the system's PV hosting capacity;
(2) Better flexible ramp-up and ramp-down capabilities can be achieved with slightly increased ESS investment costs;
(3) The idea of hierarchically placing ESSs through a centralized ESS at the substation and other distributed local ESSs is not economically preferable.

Future work will be focused on robust ESS placement to handle various scenarios of distributed generation and loads. On the other side, ESS placement will be formulated as a constrained system in future with user preference constraints on flexibility degrees. Furthermore, the approximate second-order cone relaxation is to be improved by the original AC power flow model solved through advanced global algorithms.

Author Contributions: Methodology, D.L.; Software, Y.M. and D.L.; Validation, Y.M.; Formal analysis, D.L.; Investigation, Z.J. and L.G.; Resources, L.G.; Writing—original draft, D.L.; Project administration, Z.J. All authors have read and agreed to the published version of the manuscript.

Funding: This work was funded by the State Grid Hebei Electric Power Company grant number kj2023-022.

Institutional Review Board Statement: Not applicable.

Informed Consent Statement: Not applicable.

Data Availability Statement: The data presented in this study are available on request from the corresponding author. (The data are not publicly available due to privacy restrictions.)

Conflicts of Interest: Authors Zhipeng Jing and Lipo Gao were employed by the company Economic and Technological Research Institute of State Grid Hebei Electric Power Co., Ltd. The remaining authors declare that the research was conducted in the absence of any commercial or financial relationships that could be construed as a potential conflict of interest.

Nomenclature

A. Sets

$\Omega_{b(v)}$	Set of all buses that are related to the vth FDS
Ω_T	Set of all time intervals, $\Omega_T = \{1, \cdots, T\}$
Ω_{ESS}	Set of all ESSs
Ω_{DG}	Set of all DGs
$\Omega_b \backslash \{root\}$	Set of all buses excluding the slack bus
Ω_l	Set of all lines

B. Parameters

c_{ap}	Per kWh PV curtailment cost
c_{ess}	Per kWh scheduling cost of ESSs
c_e	Per kWh investment cost of ESSs
c_g	Per kWh electricity purchasing cost
c_p	Per kW investment cost of ESSs
c_{loss}	Per kWh network loss cost
$DRR_{i,t}$	Downward ramping requirement of bus i during the tth time interval
DRR_t	Downward ramping requirement of the whole system

$I_{ij,\max}$ Capacity if line *i-j*
η_i^c Charging efficiency of the ESS at bus *i*
η_i^d Discharging efficiency of the ESS at bus *i*
$P_{i,t,\mathrm{DG}}$ Real power generation of the DG at bus *i*
$P_{i,t,\mathrm{L}}$ Real load of bus *i* during the *t*th time interval
$P_{i,t,\mathrm{NET}}$ Real net load of bus *i* during the *t*th time interval, $P_{i,t,\mathrm{NET}} = P_{i,t,\mathrm{L}} - P_{i,t,\mathrm{DG}}$.
$Q_{i,t,\mathrm{L}}$ Reactive load of bus *i* during the *t*th time interval
r_{ij} Resistance of line *i-j*
r Discount rate of ESSs
$S_{\max,\mathrm{FDS}}$ FDS's capacity
$SOC_{\min}$ Minimum state of charge of ESSs
$SOC_{\max}$ Maximum state of charge of ESSs
S_{Ti} Apparent capacity of the transformer at bus *i*
$URR_{i,t}$ Upward ramping requirement of bus *i* during the *t*th time interval
URR_t Upward ramping requirement of the whole system
$V_{\max}$, $V_{\min}$ Upper and lower bounds of $V_{i,t}$
x_{ij} Reactance of line *i-j*
y Life span of ESSs
Δt Duration (h) of each time interval

C. Variables

C_{EAI} Equivalent annual investment cost
C_{FRSC} Annual scheduling cost of ESSs
C_{NLC} Annual network power loss cost of the system
C_{Total} Annual total cost
C_{OM} Equivalent annual operation and maintenance costs of ESSs
C_{PRC} Annual electricity purchasing cost of the system from the upper-level power grid
C_{PC} Annual punishment cost for curtailment of PV generation
$E_{Ri,\mathrm{ESS}}$ Rated energy capacity of the ESS at bus *i*
$E_{i,t}$ Energy of the ESS at bus *i* during the *t*th time interval
$E_{i,0}$, $E_{i,T}$ Initial and final energy of the ESS at bus *i*
$FRD_{i,t,\mathrm{DG}}$ FRD capability of the DG at bus *i* during the *t*th time interval
$FRD_{i,t,\mathrm{ESS}}$ FRD capability of the ESS at bus *i* during the *t*th time interval
FRD_t FRD capability of the system at bus *i* during the *t*th time interval
$FRNL_i$ Fluctuation rate of real power injection at bus *i*
$FRU_{i,t,\mathrm{DG}}$ FRU capability of the DG at bus *i* during the *t*th time interval
$FRU_{i,t,\mathrm{ESS}}$ FRU capability of the ESS at bus *i* during the *t*th time interval
FRU_t FRU capability of the system at bus *i* during the *t*th time interval
$I_{ij,t}$ Current magnitude of line *i-j* during the tth time interval
$P_{i,t,\mathrm{FDS}}$ Real power injection of the FDS to bus *i* during the *t*th time interval
$P_{i,t,\mathrm{ESS}}^{+}$ Charging power of the ESS at bus *i* during the *t*th time interval
$P_{i,t,\mathrm{ESS}}^{-}$ Discharging power of the ESS at bus *i* during the *t*th time interval
$P_{Ri,\mathrm{ESS}}$ Rated charging/discharging power of the ESS at bus *i*
$P_{i,t,\mathrm{ESS}}$ Discharging power of the ESS at bus *i* during the *t*th time interval
$P_{i,t,\mathrm{ESS}}^{loss}$ Real power loss of the ESS at bus *i* during the *t*th time interval
P_t^g Real power injected from the upper-level power grid to the system during the *t*th time interval
$P_{k,t}^{\mathrm{ap}}$ Curtailed solar power at bus *k* during the *t*th time interval
$P_{i,t,\mathrm{DG}}^{\mathrm{cut}}$ Curtailed real power of the DG at bus *i*
$P_{i,t}$ Real power injection of bus *i* during the *t*th time interval
$\overline{P}_i$ Average real power injection of bus *i* during the whole period
$P_{ij,t}$ Real power of line *i-j* during the *t*th time interval
$Q_{i,t,\mathrm{FDS}}$ Reactive power injection of the FDS to bus *i* during the *t*th time interval
$Q_{i,t}$ Reactive power injection of bus *i* during the *t*th time interval
$Q_{ij,t}$ Reactive power of line *i-j* during the *t*th time interval
$\mu_{i,t}^{+}$ Binary variable indicating if the ESS at bus *i* is charging during the *t*th time interval
$\mu_{i,t}^{-}$ Binary variable indicating if the ESS at bus *i* is discharging during the *t*th time interval

σ_i	Standard deviation of real power injection at bus i
$V_{i,t}$	Voltage magnitude of bus i during the tth time interval

References

1. Grover-Silva, E.; Girard, R.; Kariniotakis, G. Optimal sizing and placement of distribution grid connected battery systems through an SOCP optimal power flow algorithm. *Appl. Energy* **2018**, *219*, 385–393. [CrossRef]
2. Zheng, Y.; Song, Y.; Huang, A.; Hill, D.J. Hierarchical optimal allocation of battery energy storage systems for multiple services in distribution systems. *IEEE Trans. Sustain. Energy* **2020**, *11*, 1911–1921. [CrossRef]
3. Su, X.; Zhang, Z.; Liu, Y.; Fu, Y.; Shahnia, F.; Zhang, C.; Dong, Z.Y. Sequential and comprehensive BESSs placement in unbalanced active distribution networks considering the impacts of BESS dual attributes on sensitivity. *IEEE Trans. Power Syst.* **2021**, *36*, 3453–3464. [CrossRef]
4. Gupta, R.; Sossan, F. Optimal sizing and siting of energy storage systems considering curtailable photovoltaic generation in power distribution networks. *Appl. Energy* **2023**, *339*, 120955. [CrossRef]
5. Cao, X.; Cao, T.; Gao, F.; Guan, X. Risk-Averse storage planning for improving RES hosting capacity under uncertain siting choices. *IEEE Trans. Sustain. Energy* **2021**, *12*, 1984–1995. [CrossRef]
6. Nick, M.; Cherkaoui, R.; Paolone, M. Optimal planning of distributed energy storage systems in active distribution networks embedding grid reconfiguration. *IEEE Trans. Power Syst.* **2018**, *33*, 1577–1590. [CrossRef]
7. Fortenbacher, P.; Ulbig, A.; Andersson, G. Optimal placement and sizing of distributed battery storage in low voltage grids using receding horizon control strategies. *IEEE Trans. Power Syst.* **2018**, *33*, 2383–2394. [CrossRef]
8. Cavus, M.; Allahham, A.; Adhikari, K.; Giaouris, D. A hybrid method based on logic predictive controller for flexible hybrid microgrid with plug-and-play capabilities. *Appl. Energy* **2024**, *359*, 122752. [CrossRef]
9. Cavus, M.; Allahham, A. Enhanced microgrid control through genetic predictive control: Integrating genetic algorithms with model predictive control for improved non-linearity and non-convexity Handling. *Energies* **2024**, *17*, 4458. [CrossRef]
10. Yi, J.H.; Cherkaoui, R.; Paolone, M. Optimal allocation of ESSs in active distribution networks to achieve their dispatchability. *IEEE Trans. Power Syst.* **2021**, *36*, 2068–2081. [CrossRef]
11. Wan, T.; Tao, Y.; Qiu, J.; Lai, S. Data-driven hierarchical optimal allocation of battery energy storage system. *IEEE Trans. Sustain. Energy* **2021**, *12*, 2097–2109. [CrossRef]
12. Gangwar, T.; Padhy, N.P.; Jena, P. Storage allocation in active distribution networks considering life cycle and uncertainty. *IEEE Trans. Ind. Inform.* **2023**, *19*, 339–350. [CrossRef]
13. Wang, B.; Zhang, C.; Dong, Z.Y.; Li, X. Improving hosting capacity of unbalanced distribution networks via robust allocation of battery energy storage systems. *IEEE Trans. Power Syst.* **2021**, *36*, 2174–2185. [CrossRef]
14. Bozorgavari, S.A.; Aghaei, J.; Pirouzi, S.; Nikoobakht, A.; Farahmand, H.; Korpas, M. Robust planning of distributed battery energy storage systems in flexible smart distribution networks: A comprehensive study. *Renew. Sustain. Energy Rev.* **2020**, *123*, 109739. [CrossRef]
15. Awad, A.S.A.; El-Fouly, T.H.M.; Salama, M.M.A. Optimal ESS allocation for benefit maximization in distribution networks. *IEEE Trans. Smart Grid* **2017**, *8*, 1668–1678. [CrossRef]
16. Santos, S.F.; Fitiwi, D.Z.; Shafie-Khah, M.; Bizuayehu, A.W.; Cabrita, C.M.P.; Catalao, J.P.S. New multistage and stochastic mathematical model for maximizing RES hosting capacity-part I: Problem formulation. *IEEE Trans. Sustain. Energy* **2017**, *8*, 304–319. [CrossRef]
17. Wu, X.; Conejo, A.J.; Mathew, S. Optimal siting of batteries in distribution systems to enhance reliability. *IEEE Trans. Power Deliv.* **2021**, *36*, 3118–3127. [CrossRef]
18. Inaolaji, A.; Wu, X.; Roychowdhury, R.; Smith, R. Optimal allocation of battery energy storage systems for peak shaving and reliability enhancement in distribution systems. *J. Energy Storage* **2024**, *95*, 112305. [CrossRef]
19. Oraibi, W.A.; Mohammadi-Ivatloo, B.; Hosseini, S.H.; Abapour, M. A resilience-oriented optimal planning of energy storage systems in high renewable energy penetrated systems. *J. Energy Storage* **2023**, *67*, 107500. [CrossRef]
20. Das, C.K.; Bass, O.; Mahmoud, T.S.; Kothapalli, G.; Mousavi, N.; Habibi, D.; Masoum, M.A.S. Optimal allocation of distributed energy storage systems to improve performance and power quality of distribution networks. *Appl. Energy* **2019**, *252*, 113468. [CrossRef]
21. Ghaffari, A.; Askarzadeh, A.; Fadaeinedjad, R. Optimal allocation of energy storage systems, wind turbines and photovoltaic systems in distribution network considering flicker mitigation. *Appl. Energy* **2022**, *319*, 119253. [CrossRef]
22. Khajeh, H.; Parthasarathy, C.; Doroudchi, E.; Laaksonen, H. Optimized siting and sizing of distribution-network-connected battery energy storage system providing flexibility services for system operators. *Energy* **2023**, *285*, 129490. [CrossRef]
23. Wang, Q.; Hodge, B.-M. Enhancing power system operational flexibility with flexible ramping products: A review. *IEEE Trans. Ind. Inform.* **2017**, *13*, 1652–1664. [CrossRef]